The Canadian Mineralogist
Vol. 44, pp. 1089-1097 (2006)

SOLID SOLUTIONS OF NIOBIUM IN SYNTHETIC TITANITE

RUSLAN P. LIFEROVICH AND ROGER H. MITCHELL¶

Department of Geology, Lakehead University, 955 Oliver Road, Thunder Bay, Ontario P7B 5E1, Canada

ABSTRACT

Synthetic $(Ca_{1-x}Na_x)(Ti_{1-x}Nb_x)OSiO_4$ and $Ca(Ti_{1-2x}Nb_xAl_x)OSiO_4$ solid solutions have been prepared for $x = 0.1$ and 0.2 by ceramic methods and their crystal structure determined by Rietveld analysis. At ambient conditions, the isomorphic capacity of (F,OH)-free titanite is ~0.25 *apfu* Nb in a single-site scheme of substitution ($2\,^{VI}Ti^{4+} \rightleftharpoons {}^{VI}Al^{3+} + {}^{VI}Nb^{5+}$) and ~0.22 *apfu* Nb in a two-site scheme ($^{VII}Ca^{2+} + {}^{VI}Ti^{4+} \rightleftharpoons {}^{VII}Na^{+} + {}^{VI}Nb^{5+}$). All cations located at the ^{VII}X and ^{VI}Y sites are disordered. Analysis of tetrahedron bond-lengths indicates the absence of Al^{3+} replacing Si^{4+} in coordination tetrahedra. All Nb-doped varieties of titanite adopt space group *A*2/*a*. Thus, both single-site and complex multivalent schemes of substitution destroy the coherence of the off-centering of chains of octahedra typical of the $CaTiOSiO_4$ end member, resulting in a $P2_1/a \rightarrow A2/a$ phase transition. The $(Ca_{1-x}Na_x)(Ti_{1-x}Nb_x)OSiO_4$ scheme of substitution incorporates the larger cations at both the ^{VII}X and ^{VI}Y sites, whereas the $Ca(Ti_{1-2x}Nb_xAl_x)OSiO_4$ scheme involves only ^{VI}Y-site (Al^{3+}, Nb^{5+}) cations, with a slightly smaller "average" radius. Unit-cell dimensions change insignificantly and vary sympathetically with the change of average radii of the cations in the $(Ca_{1-x}Na_x)(Ti_{1-x}Nb_x)OSiO_4$ series and vary insignificantly in the $Ca(Ti_{1-2x}Nb_xAl_x)OSiO_4$ series. Both Nb-doped titanite and pure $CaTiOSiO_4$ consist of distorted polyhedra. The seven-fold coordination polyhedra and octahedra in Nb-doped titanite are slightly less stretched as compared to those in pure $CaTiOSiO_4$. The SiO_4 tetrahedron is compressed in Nb-doped titanite as compared to that in the pure $CaTiOSiO_4$. The experimental data obtained suggest that the existence of a titanite analogue with more than 50 mol.% of $NaNbOSiO_4$ end member is unlikely. The solid solution involving the smaller ^{VI}(Al,Nb) cations theoretically could be stabilized at high pressure, suggesting the existence of a potentially new species dominated by the $Ca(AlNb)OSiO_4$ end member. The synthetic titanite compositions may be suitable for the sequestration of radioactive waste containing ^{94}Nb.

Keywords: titanite, Rietveld analysis, crystal structure, distortion, niobium, aluminum, sodium, radwaste disposal.

SOMMAIRE

Nous avons synthétisé les solutions solides $(Ca_{1-x}Na_x)(Ti_{1-x}Nb_x)OSiO_4$ et $Ca(Ti_{1-2x}Nb_xAl_x)OSiO_4$ (x égal à 0.1 et 0.2) par méthodes céramiques, et nous avons déterminé leur structure cristalline par la méthode Rietveld. A conditions ambiantes, la capacité de la titanite stoechiométrique à accepter le Nb est environ ~0.25 *apfu* Nb dans un schéma impliquant un seul site ($2\,^{VI}Ti^{4+} \rightleftharpoons {}^{VI}Al^{3+} + {}^{VI}Nb^{5+}$) et environ ~0.22 *apfu* Nb dans un schéma impliquant deux sites ($^{VII}Ca^{2+} + {}^{VI}Ti^{4+} \rightleftharpoons {}^{VII}Na^{+} + {}^{VI}Nb^{5+}$). Tous les cations situés sur les sites ^{VII}X et ^{VI}Y sites sont désordonnés. Une analyse des longueurs des liaisons des tétraèdres montre que Al^{3+} ne remplace pas Si^{4+}. Toutes les préparations de titanite contenant le Nb adoptent le groupe d'espace *A*2/*a*. Ainsi, les deux schémas de substitution, impliquant un seul site ou deux sites, détruisent la cohérence des déplacements dans les chaînes d'octaèdres de la titanite idéale $CaTiOSiO_4$, provoquant ainsi une inversion de $P2_1/a$ à $A2/a$. Dans le schéma de substitution $(Ca_{1-x}Na_x)(Ti_{1-x}Nb_x)OSiO_4$, les plus gros cations sont incorporés aux deux sites, ^{VII}X et ^{VI}Y, tandis que dans le cas du schéma $Ca(Ti_{1-2x}Nb_xAl_x)OSiO_4$, les cations ($Al^{3+}$, Nb^{5+}) sont uniquement sur le site ^{VI}Y, qui possède un rayon moyen un peu plus petit. Les paramètres réticulaires varient de façon très mineure selon le changement en rayon ionique moyen des cations dans la série $(Ca_{1-x}Na_x)(Ti_{1-x}Nb_x)OSiO_4$, et encore moins dans la série $Ca(Ti_{1-2x}Nb_xAl_x)OSiO_4$. La titanite dopée en Nb et la titanite pure $CaTiOSiO_4$ contiennent des polyèdres de coordinence difformes. Les polyèdres à coordinence sept et les octaèdres dans la titanite dopée au Nb sont légèrement moins étirés que ceux dans le $CaTiOSiO_4$ pur. Le tétraèdre SiO_4 est comprimé dans la titanite dopée au Nb en comparaison du tétraèdre dans le $CaTiOSiO_4$ pur. Les données expérimentales obtenues semblent indiquer qu'un analogue de la titanite ayant plus de 50% (base molaire) du pôle $NaNbOSiO_4$ n'est probablement pas stable. La solution solide impliquant les cations plus petits ^{VI}(Al,Nb) pourrait en théorie être stabilisée à pression élevée, ce qui laisse prévoir une nouvelle espèce ayant comme pôle $Ca(AlNb)OSiO_4$. Les compositions synthétiques de titanite pourraient être appropriées pour la séquestration de déchêts radioactifs contenant le ^{94}Nb.

(Traduit par la Rédaction)

Mots-clés: titanite, analyse Rietveld, structure cristalline, distorsion, niobium, aluminium, sodium, déchêts radioactifs.

¶ *E-mail address*: rmitchel@lakeheadu.ca

Introduction

Niobium is a common minor constituent of natural titanite, $^{VII}X\ ^{VI}Y OSiO_4$, where X = Ca, Na, *REE*, Y, Sr, Mn, and Y = Ti, Sn, Sb, Al, Fe, Zr, Ta, Nb (Sahama 1946, Černý & Riva di Sanseverino 1972, Paul *et al.* 1981, Sawka *et al.* 1984, Della Ventura *et al.* 1999, Tiepolo *et al.* 2002, Chakhmouradian & Zaitsev 2002, Chakhmouradian *et al.* 2003, Chakhmouradian 2004). Entry of Nb^{5+} into the titanite structure at the ^{VI}Y site is commonly balanced by $(Al,Fe)^{3+}$ or by the replacement of Ca^{2+} by Na^{+} at the ^{VII}X site. Charge-balancing substitutions of O^{2-} by $(F,OH)^{-}$ involving the anionic site O(1) also are possible. The most strongly niobian varieties of titanite are known to crystallize from the latest-forming low-temperature derivatives of alkaline rocks (Chakhmouradian 2004) and can contain up to 16.4 wt.% Nb_2O_5 [0.25 *apfu* Nb (Liferovich & Mitchell 2005a)].

Data on the crystal structure of naturally occurring Nb-rich titanite are limited to a single-crystal study of titanite from Mt. Somma, Italy containing 0.04 *apfu* Nb, and comparable amounts of Zr, OH and F. These data suggest that a single-site diadochy, $2Ti^{4+} \rightleftharpoons (Al,Fe)^{3+} + Nb^{5+}$, is primarily responsible for the incorporation of Nb at the ^{VI}Y site (Brigatti *et al.* 2004). A study of the structure of Nb-rich naturally occurring titanite is typically hindered by significant compositional inhomogeneity (Chakhmouradian 2004, Liferovich & Mitchell 2005a). For this reason, we have synthesized and refined the crystal structure of the compositional analogue of natural titanite containing 0.15 *apfu* Nb, which involves a two-site cationic scheme of substitution: $^{VII}Ca^{2+} + 2\,^{VI}Ti^{4+} \rightleftharpoons {}^{VII}Na^{+} + {}^{VI}Nb^{5+} + {}^{VI}Zr^{4+}$ (Liferovich & Mitchell 2005a). Such a complex two-site substitution might permit the entry of more Nb into the structure than would be possible with a single-site substituted material.

In this contribution, we present experimental data regarding the synthesis of Nb-rich titanite together with observations on the response of the structure to single-site and two-site substitutions involving Nb.

The Crystal Structure and Phase Transitions of Titanite: An Overview

The structure of titanite consists of kinked chains of corner-linked YO_4O_2 octahedra sharing O(1) atoms (Fig. 1). The SiO_4 tetrahedra cross-link the chains of octahedra. Irregular XO_7 polyhedra form interlacing chains sharing edges *via* couples of oxygen atoms; these chains extend down [101]. The YO_6 and XO_7 chains are interconnected by shared edges. The titanite structure can be considered as a $[YOSiO_4]^{2-}$ framework

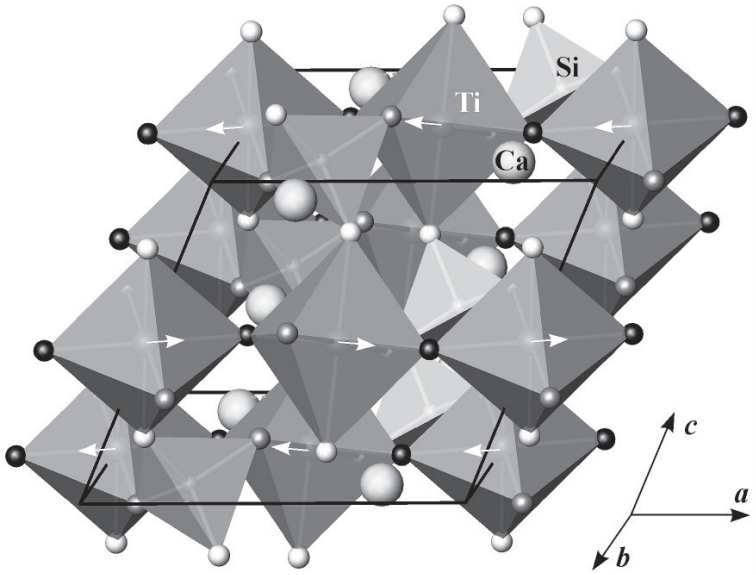

FIG. 1. Crystal structure of titanite. Lines represent the unit-cell boundaries. Arrows within TiO_6 octahedra represent off-center displacement of six-coordinated atoms from the ideal position observed in the $CaTiOSiO_4$, which disappears in the Na–Nb- and Nb–Al-doped synthetic titanite. The O(1), O(2) and O(3) atoms are shown as small black, light grey and grey spheres, respectively.

with large cavities enclosing *X* atoms (essentially Ca) in irregular seven-fold cages (Speer & Gibbs 1976, Taylor & Brown 1976).

At ambient conditions, in $CaTiOSiO_4$, all ^{VI}Ti atoms occur in off-center positions that are displaced in the same direction within an individual TiO_6 chain, but in opposite directions between neighboring chains, resulting in $P2_1/a$ symmetry. According to Kunz & Brown (1994), this displacement of ^{VI}Ti atoms "out of their otherwise regular octahedron coordination" is caused by an electronic second-order Jahn–Teller effect occurring around the octahedrally coordinated cations of this d^0 transition metal. Kek *et al*. (1997) considered ordering of Ca in the ^{VII}X site as another trigger of the antiferroelectric displacement of ^{VI}Ti in the low-temperature $CaTiOSiO_4$.

The $P2_1/a$ to $A2/a$ phase transition in titanite can be induced by either an increase in pressure or temperature (Kunz *et al*. 1996, 2000, Kek *et al*. 1997, Angel *et al*. 1999), or occurs as a structural response to elemental substitutions involving the single YO_6 site, or complex substitutions at the YO_6 + O(1) or XO_7 + YO_6 sites (Higgins & Ribbe 1976, Speer & Gibbs 1976, Troitzsch & Ellis 2002).

Group-theoretical considerations for the $CaTiOSiO_4$ end-member allow stepwise changes in symmetry from $P2_1/a$ ($P2_1/n$ in conventional settings) to $A2/a$ ($C2/c$) *via* an intermediate disordered phase (Kek *et al*. 1997). The complete transformation results in centering of the octahedrally coordinated atoms in the YO_6 polyhedra due to equalization of the *Y*–O(1) and *Y*–O(1)' distances at P ≥ 3.5 GPa or T > 825 K (Kunz *et al*. 2000, Malcherek 2001, among others), and in oscillations of the ^{VII}X atom between two positions (Kek *et al*. 1997). An intermediate non-quenchable transition between 496 and 825 K (Ghose *et al*. 1991, Van Heurk *et al*. 1991, Salje *et al*. 1993) results from loss of long-range order and creation of antiphase boundaries between O(1)–*Y*–O(1)' dipoles, leaving domains of $P2_1/a$ symmetry on the unit-cell scale, but an overall, pseudocentered $A2/a$ symmetry on a long-range scale (Taylor & Brown 1976, Higgins & Ribbe 1976, Speer & Gibbs 1976, Kunz *et al*. 1996, Hughes *et al*. 1997, Troitzsch *et al*. 1999). The ^{VII}X atom is on a split position in this intermediate phase (Kek *et al*. 1997). Troitzsch & Ellis (2002) referred to the low-temperature phase with space group $P2_1/a$ as α, the intermediate $A2/a$ phase as β, and the high-P, high-T phase with true $A2/a$ symmetry as γ titanite. A further temperature-driven phase transition is possible above 1150 K (Chrosch *et al*. 1997). Conventionally, the α → β modification is referred to as "the $P2_1/a$ to $A2/a$ phase transition", bearing in mind that it probably does not strictly represent the entire $P2_1/a \rightarrow A2/a$ transformation (Troitzsch & Ellis 2002).

In pure $CaTiOSiO_4$, different types of polyhedra have different responses to distortions induced by both high pressure and high temperature. The SiO_4 tetrahedra show a strong angular distortion with only minor change in bond lengths, whereas the polymerized CaO_7 polyhedra are significantly distorted, and TiO_6 octahedra rotate rigidly (Kunz *et al*. 2000).

Compositionally driven phase-transitions in titanite are similar to those driven by high pressure or high temperature (Troitzsch & Ellis 2002, and references therein). Doping of the YO_6 site with the smaller Al^{3+} ions, balanced by $(F,OH)^-$ at the O(1) site, results in the α → β transition at low Al + (F,OH) contents and a further "β → γ"-like modification in more Al-rich titanite (Troitzsch & Ellis 2002). Stabilization of β titanite is possible at ambient conditions by means of two-site substitutions involving as little as 5 mol.% $^{VI}Al^{3+}$ coupled with 5 mol.% charge-balancing $^{VII}Dy^{3+}$ (Hughes *et al*. 1997), whereas in the case of substitutions involving octahedrally coordinated cations balanced by an equal amount of F^- at the O(1) site, the β dimorph becomes stable in the range of 9–18.2 mol.% $^{VI}Al^{3+}$ (Troitzsch *et al*. 1999). This difference is due to relief of the underbonding of the bridging O(1) anions at antiphase boundaries, created in response to long-range disorder, and stabilization of the β form of titanite is more easily induced by substitutions at the seven-fold site (Hughes *et al*. 1997).

Here, we provide data on the response of the (OH,F)-free titanite structure to the entry of Nb with concomitant multivalent substitutions at the octahedral site or in the seven-fold site. These schemes of substitution have been investigated for the synthetic series $(Ca_{1-x}Na_x)(Ti_{1-x}Nb_x)OSiO_4$ and $Ca(Ti_{1-2x}Nb_xAl_x)OSiO_4$ (x = 0.1 and 0.2). Studies of other schemes of substitution involving Nb, as well as Ta, are in progress.

Experimental and Analytical Techniques

For consistency, we tried to prepare all samples by the same solid-state ceramic techniques from stoichiometric amounts of $CaSiO_3$ (wollastonite polymorph 1*A*), TiO_2, Nb_2O_5, Al_2O_3, and Na_2CO_3. The reagents, dried at 120°C for several days, were mixed, ground in an agate mortar under acetone, and calcined in air for 24 h at 1000°C. After regrinding for 1 h, the samples were pelletized at a pressure of 10 tonnes per cm^2, and then heated in air for 96 h at 1175°C with further grinding (and pellet preparation) after the first 48 h and quenching in air. The crystal-structure parameters of the synthetic $CaTiOSiO_4$ obtained by this method of synthesis are close to those obtained from synchrotron data given by Kek *et al*. (1997) for $CaTiOSiO_4$ (Liferovich & Mitchell 2005b). Homogeneous samples of Al–Nb-doped titanite were prepared in this manner. Homogeneous Na–Nb-doped titanite was not formed during 96 hours of solid-state reaction. Longer-duration sintering resulted in volatilization of Na. The successful synthesis of the Na–Nb-doped titanite was performed by melting the samples at 1225°C for ½ hour. The samples subjected to melting contained 5% excess of Na after pre-sintering as described above. The melted

samples were cooled to 1175°C, and then sintered for 24 hours followed by quenching. Homogeneous products were obtained for $Ca_{0.9}Na_{0.1}Ti_{0.9}Nb_{0.1}OSiO_4$ and $Ca_{0.8}Na_{0.2}Ti_{0.8}Nb_{0.2}OSiO_4$.

The synthetic materials were investigated by energy-dispersion X-ray spectrometry (EDXA) using a JEOL JSM–5900 scanning electron microscope equipped with a Link ISIS 300 analytical system. Raw EDS spectra were acquired for 130 s (live time) with an accelerating voltage of 20 kV, and beam current of 0.475 nA. The spectra were processed with the LINK ISIS–SEMQUANT quantitative software package, with full ZAF corrections applied. The following well-characterized minerals and synthetic compounds were used as analytical standards: ilmenite (Ti), corundum (Al), wollastonite (Ca), pyroxene glass DJ35 (Si), loparite (Nb), and jadeite (Na). The accuracy of Na analysis was cross-checked by the control compositions of natural natrolite and analcime.

Powder X-ray-diffraction (XRD) patterns were obtained at room temperature using a Philips 3710 diffractometer (T = 20°C; Cu$K\alpha$ radiation; 2θ range 9°–145°, Δ2θ step 0.02° per 4 s). The patterns were analyzed by the Rietveld method using the Bruker AXS software TOPAS 2.1 (Kern & Coelho 1998). In addition, high-resolution XRD patterns were obtained in the 2θ range 31.7°–33.4° (Δ2θ step 0.005°; counting time per step: 30 s).

The ATOMS 6.0 software (Dowty 1999) was used to determine framework angles and interaxial angles for calculation of indices of bond-angle variation. The IVTON program (Balić-Žunić & Vicković 1996) was employed to obtain selected bond-lengths and to characterize the coordination spheres of the cations.

Results and Discussion

The samples of sodic niobian and aluminian niobian titanite synthesized here consist of fine-grained aggregates with average grain-size of 10–15 μm, containing very little amount of by-products (1.5–3.4 wt.% in total). Some of the SiO_2 impurity is considered to have been introduced by use of an agate mortar during sample preparation.

Synthesis of the entire $(Ca_{1-x}Na_x)(Ti_{1-x}Nb_x)OSiO_4$ and $Ca(Ti_{1-2x}Nb_xAl_x)OSiO_4$ series was attempted, but was successful only for the compositional range of x = 0.1 and 0.2. No significant compositional heterogeneity was revealed by back-scattered electron (BSE) imagery for the compounds with x = 0.1 and 0.2 in both series.

For experiments with $x > 0.2$, SEM BSE images and XRD patterns reveal conspicuous compositional heterogeneity and demonstrate the presence of wollastonite (transformed to the 4*A* polymorph), rutile, complex titanates, and niobates. In addition, the amount of starting material remaining as non-reacted phases increases with x. The titanium-free end-member compounds with x = 1 did not form any titanite-structured phases. SEM EDXA data for run products obtained for $0 \le x \le 0.2$ agree well with results for refinements of ^{VII}X and ^{VI}Y site-occupancies for the same samples using the Rietveld technique. The most niobian composition of the titanite obtained for runs with $x > 0.3$ in the $Ca(Ti_{1-2x}Nb_xAl_x)OSiO_4$ series is (wt.% [*apfu* cation]): 5.6 [0.22] Al_2O_3, 27.6 [0.93] SiO_2, 27.6 [0.99] CaO, 23.5 [0.6] TiO_2, and 16.5 [0.25] Nb_2O_5, total 100.8 [3.0]. These data indicate that $x \approx 0.25$ *apfu* Nb is the empirical limit for diadochy between Nb and Ti in the octahedral site of the (F,OH)-free structure at ambient conditions. Crystal structures of titanite samples produced in runs with $x > 0.2$ are not considered here because the results of our refinements are not robust owing to the presence of significant amounts of impurities.

Rietveld refinement

For the Nb-doped varieties of titanite synthesized, powder X-ray diffractometry does not demonstrate the presence of $2\bar{2}1$ and $2\bar{1}2$ reflections, which occur clearly in the high-resolution XRD pattern of the pure $CaTiOSiO_4$ end member (Fig. 2). Given that extinction rules do not allow the $k + l$ = odd reflections in the space group *A*2/*a* (Taylor & Brown 1976, Hollabaught & Foit 1984, Kunz *et al.* 1996), we conclude that doping of titanite with Nb at ambient pressure according to either the single- or two-site scheme of substitution results in the stabilization of an *A*2/*a* dimorph in accordance with constraints maintained for titanite structure by group-theoretical considerations (Kek *et al.* 1997).

For Rietveld refinement of the *A*2/*a*-structured Nb-bearing varieties of titanite, we used as starting parameters the atom coordinates given by Mongiorgi & Riva di Sanseverino (1968). Figure 2 is a portion of the Rietveld refinement plot for the synthetic $CaTi_{0.6}Al_{0.2}Nb_{0.2}OSiO_4$ titanite ("$AlNb_2$") over the 2θ range from 15 to 100° (note that the actual refinement is over the 9–145° 2θ range).

Agreement factors and crystal-structure parameters for Nb-bearing sodic and aluminian titanite are listed in Table 1 in comparison with crystal-structure parameters calculated for $CaTiOSiO_4$ on the basis of synchrotron radiation data published by Kek *et al.* (1997). Positional parameters and thermal parameters of the atoms obtained for Nb-bearing titanite are listed in Table 2. Selected bond-lengths are given in Table 3. All cations located at the ^{VII}X and ^{VI}Y sites are disordered. Refinement of the site occupancies shows no vacancies at cationic sites within the accuracy of the Rietveld results.

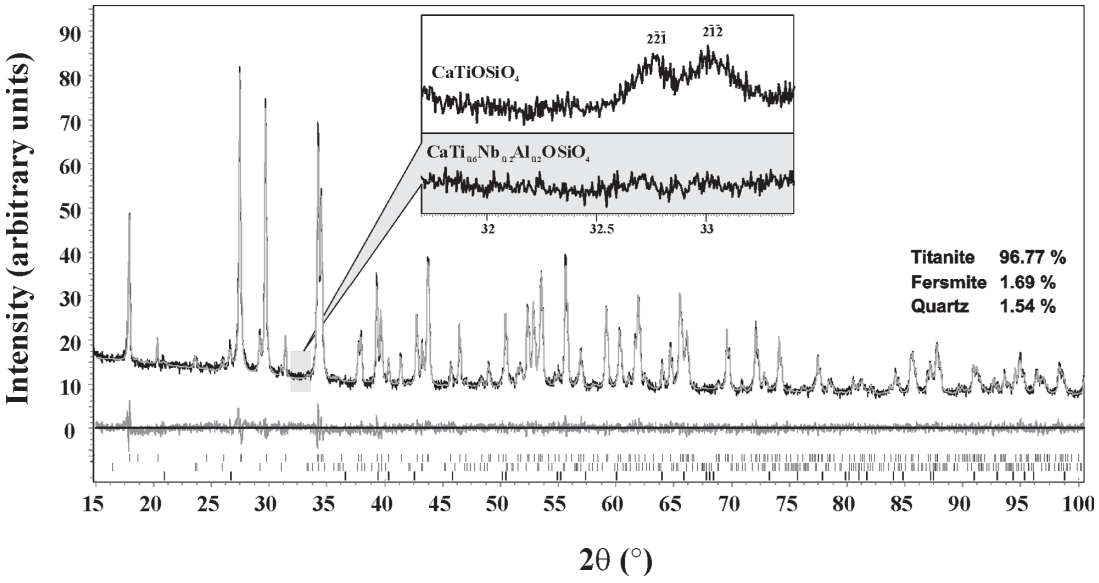

FIG. 2. Rietveld refinement plot of the X-ray powder-diffraction data for synthetic titanite $CaTi_{0.6}Nb_{0.2}Al_{0.2}OSiO_4$ at room temperature. For details of the refinement, see text and Table 2.

Geometry of sites in Nb-rich aluminous and sodic titanite

The $(Ca_{1-x}Na_x)(Ti_{1-x}Nb_x)OSiO_4$ scheme of substitution incorporates slightly larger cations at both the ^{VII}X and ^{VI}Y sites, whereas the $Ca(Ti_{1-2x}Nb_xAl_x)OSiO_4$ scheme involves only (Al^{3+},Nb^{5+}) cations with a slightly smaller "average" radius (Shannon 1976) at the ^{VI}Y site. Unit-cell dimensions change insignificantly in varieties of Nb-rich titanite and vary sympathetically with average radii of cations at the ^{VII}X and ^{VI}Y sites in the $(Ca_{1-x}Na_x)(Ti_{1-x}Nb_x)OSiO_4$ series. In the case of the $Ca(Ti_{1-2x}Nb_xAl_x)OSiO_4$ series, these variations are negligible (Table 1).

The mean cation–oxygen distances within the XO_7 and YO_6 coordination polyhedra vary insignificantly (Table 1). The <*X*–O> distances are statistically very similar for all the varieties of titanite obtained here and pure $CaTiOSiO_4$ described by Kek *et al*. (1997) and Liferovich & Mitchell (2005b). Entry of Nb^{5+} at the ^{VI}Y site, being slightly larger than Ti^{4+} [$^{VI}R = 0.64$ and 0.605 Å, respectively (Shannon 1976)], does not affect the <*Y*–O> distances in the Na–Nb-doped titanite. The <*Y*–O> distances decrease in the Nb–Al-doped titanite owing to entry at the ^{VI}Y site of $(Al_{0.5},Nb_{0.5})$, with an average cationic radius slightly smaller than that of Ti^{4+} [$^{VI}R_{(0.5Al+0.5Nb)} = 0.59$ Å].

The volume of the SiO_4 tetrahedron and the mean <Si–O> bond-length in the Nb-bearing varieties of titanite are less than those in the $CaTiOSiO_4$ end member (Table 1). The dimensions of the SiO_4 tetrahedron decrease stepwise with the double-site substitution $^{VII}Na^+ + {}^{VI}Nb^{5+} \rightleftharpoons {}^{VII}Ca^{2+} + {}^{VI}Ti^{4+}$ (Table 1), and do not change with x in the case of single-site substitution $^{VI}Al^{3+} + {}^{VI}Nb^{5+} \rightleftharpoons 2^{VI}Ti^{4+}$. Observed deviations of the mean bond-lengths from those in the Al-free SiO_4 tetrahedron are conventionally used for considering possible substitutions of the larger Al^{3+} for the smaller Si^{4+} [$^{IV}R_{Al^{3+}} = 0.39$, $^{IV}R_{Si^{4+}} = 0.26$ Å (Shannon 1976)] at the tetrahedral site(s) of various silicates and aluminosilicates. A quantitative model has not yet been developed for infinite framework-type structure(s) containing tetrahedra and octahedra such as titanite, although some semiquantitative comparisons with well-studied tectosilicates seem possible. Thus, the <Si–O> distances in completely ordered anorthite range from 1.608 to 1.617 Å, whereas the <Al–O> distances range from 1.742 to 1.755 Å (Wainwright & Starkey 1971, Ghose *et al*. 1993). Similar mean <Si–O> distances are found in the following ordered aluminosilicates: lisetite: 1.619 Å, 1.620 Å, 1.622 Å and 1.623 Å (Rossi *et al*. 1986), slawsonite: 1.624 Å (Griffen *et al*. 1977), paracelsian: 1.613 Å (Chiari *et al*. 1985), nepheline: 1.603–1.616 Å (Tait *et al*. 2003), stronalsite: 1.609 and 1.619 Å (Liferovich et al. 2006), and banalsite: 1.621 and 1.622 Å (Liferovich *et al*. 2006). Hence, the similarity of the <*T*–O> distances for the $AlNb_1$ and $AlNb_2$ samples [1.618(9) and 1.621(10) Å, respectively; Table 1] to <Si–O> bond lengths in completely ordered tectosilicates implies the absence of Si ⇌ Al substitution at the tetrahedral site in the niobian–aluminian varieties of titanite.

TABLE 1. RIETVELD REFINEMENT RESULTS AND CRYSTAL-STRUCTURE PARAMETERS

	$CaTiOSiO_4$*	$NaNb_1$	$NaNb_2$	$AlNb_1$	$AlNb_2$
a, Å	7.0697(3)	7.0815(1)	7.0952(1)	7.0571(1)	7.0594(1)
b, Å	8.7223(4)	8.7175(1)	8.7172(2)	8.7169(1)	8.7188(1)
c, Å	6.5654(4)	6.5750(1)	6.5824(1)	6.5630(1)	6.5651(1)
ß, °	113.853(4)	113.915(1)	113.982(1)	113.756(1)	113.747(1)
V, Å³	370.27(1)	371.05(1)	371.98(1)	369.52(1)	369.86(1)
R_{wp}, %		12.46	12.48	10.95	10.54
R_{Bragg}, %		3.80	5.17	3.41	3.58
GoF		1.39	1.50	1.36	1.42
DW		1.16	0.96	1.17	1.09
<*X*-O>, Å	2.457(1)	2.461(12)	2.475(15)	2.454(11)	2.462(12)
V_{XO7}, Å³	19.662	19.928	20.393	19.791	19.974
Δ_7	2.42	2.115	1.535	2.19	1.75
υ_7	0.162	0.155	0.151	0.154	0.154
<*Y*-O>, Å	1.959(1)	1.975(8)	1.974(8)	1.971(7)	1.963(8)
V_{YO6}, Å³	9.969	10.246	10.222	10.176	10.062
d_Y	0.113				
∂_{xY}	0.015				
∂_{yY}	0.004				
∂_{zY}	0.0				
Δ_6	2.20	1.34	1.57	1.33	1.31
υ_6	0.002	0.003	0.003	0.003	0.003
δ_6	9.40	2.06	2.23	2.00	1.85
<Si-O>, Å	1.647(1)	1.621(9)	1.614(11)	1.618(9)	1.621(10)
V_{SiO4}, Å³	2.283	2.172	2.140	2.154	2.168
Δ_4	0.002	0.02	0.03	0.05	0.05
υ_4	0.005	0.007	0.008	0.009	0.009
δ_4	12.66	15.86	17.80	18.54	20.67
Y-O1-*Y*, °	141.5	141.7	144.2	141.39	142.7
Si-O2-*Y*, °	144.6	141.1	141.2	141.3	141.4
Si-O3-*Y*, °	138.4	127.6	128.6	128.3	129.0
Si-O4-*Y*, °	128.7				
Si-O5-*Y*, °	125.1				

* Synchrotron radiation data for $P2_1/a$-structured $CaTiSiO_5$ (Kek *et al.* 1997).

Nb-doped synthetic titanite: $NaNb_1$: $Ca_{0.9}Na_{0.1}Ti_{0.9}Nb_{0.1}OSiO_4$; $NaNb_2$: $Ca_{0.8}Na_{0.2}Ti_{0.8}Nb_{0.2}OSiO_4$; $AlNb_1$: $CaTi_{0.8}Al_{0.1}Nb_{0.1}OSiO_4$; $AlNb_2$: $CaTi_{0.6}Al_{0.2}Nb_{0.2}OSiO_4$.

d_Y: The displacement of the central atom; ∂_{xY}, ∂_{yY} and ∂_{zY} components of the vector of ^{VI}Y atom displacement; Δ_n: polyhedron bond-length distortion, equal to:

$1/n \bullet \Sigma\{(r_i - \bar{r}) / \bar{r}\}^2 \bullet 10^3$, where r_i and $\bar{r}$ are individual and average bond-lengths, respectively (Shannon 1976).

υ_n: Polyhedron-volume distortion calculated relative to an ideal polyhedron with the same coordination number and inscribed in the sphere with the radius r_x [average distance from centroid to ligands (Makovicky & Balić-Žunić 1998, Balić-Žunić & Vicković 1996)].

δ_n: Bond-angle variance for the regular polyhedra, $\delta_n = \Sigma[(\theta_i - \varphi_j)^2/(n-1)]$, where θ_i are bond-angles and φ_j is an ideal bond-angle (Robinson *et al.* 1971).

Parameters for $P2_1/a$-structured compound are given in the second column.

TABLE 2. POSITIONAL AND THERMAL PARAMETERS FOR STOICHIOMETRIC TITANITE AND Nb-DOPED SYNTHETIC TITANITE

Position	Sample	*x*	*y*	*z*	B_{iso} [Å²]
^{VII}X	$CaTiOSiO_4$*	0.2414(1)	0.4184(0)	0.2512(0)	
	$NaNb_1$	¼	0.1685(3)	0	1.01(8)
	$NaNb_2$	¼	0.1691(4)	0	0.65(10)
	$AlNb_1$	¼	0.1693(2)	0	1.38(7)
	$AlNb_2$	¼	0.1697(3)	0	1.42(8)
^{VI}Y	$CaTiOSiO_4$*	0.5148(1)	0.2544(2)	0.7494(0)	
	$NaNb_1$	½	0	½	0.52(4)
	$NaNb_2$	½	0	½	0.78(5)
	$AlNb_1$	½	0	½	0.68(4)
	$AlNb_2$	½	0	½	0.76(4)
^{IV}Si	$CaTiOSiO_4$*	0.7481(0)	0.4329(1)	0.2488(0)	
	$NaNb_1$	¾	0.1815(4)	0	0.36(8)
	$NaNb_2$	¾	0.1800(5)	0	0.22(10)
	$AlNb_1$	¾	0.1810(4)	0	0.51(7)
	$AlNb_2$	¾	0.1809(4)	0	0.42(7)
O1	$CaTiOSiO_4$*	0.7494(1)	0.3208(1)	0.7495(1)	
	$NaNb_1$	¾	0.0705(6)	½	0.55(6)
	$NaNb_2$	¾	0.0658(7)	½	0.39(7)
	$AlNb_1$	¾	0.0709(6)	½	0.83(6)
	$AlNb_2$	¾	0.0683(6)	½	0.77(6)
O2	$CaTiOSiO_4$*	0.9105(1)	0.3163(1)	0.4346(1)	
	$NaNb_1$	0.9102(6)	0.0671(4)	0.1812(6)	0.55(6)
	$NaNb_2$	0.9112(7)	0.0682(5)	0.1816(7)	0.39(7)
	$AlNb_1$	0.9073(6)	0.0656(4)	0.1796(5)	0.83(6)
	$AlNb_2$	0.9085(6)	0.0660(4)	0.1807(6)	0.77(6)
O3	$CaTiOSiO_4$*	0.0869(1)	0.1842(1)	0.0630(1)	
O4	$CaTiOSiO_4$*	0.3838(1)	0.4608(1)	0.6469(1)	
O3	$NaNb_1$	0.3828(7)	0.2137(4)	0.4001(7)	0.55(6)
	$NaNb_2$	0.3849(8)	0.2152(5)	0.4048(8)	0.39(7)
	$AlNb_1$	0.3833(6)	0.2126(4)	0.4014(6)	0.83(6)
	$AlNb_2$	0.3862(6)	0.2123(4)	0.4050(7)	0.77(6)
O5	$CaTiOSiO_4$*	0.6186(1)	0.0402(1)	0.8534(1)	

* Synchrotron radiation data for $P2_1/a$-structured $CaTiSiO_5$ (Kek *et al.* 1997).
Nb-doped synthetic titanite: $NaNb_1$: $Ca_{0.9}Na_{0.1}Ti_{0.9}Nb_{0.1}OSiO_4$; $NaNb_2$: $Ca_{0.8}Na_{0.2}Ti_{0.8}Nb_{0.2}OSiO_4$; $AlNb_1$: $CaTi_{0.8}Al_{0.1}Nb_{0.1}OSiO_4$; $AlNb_2$: $CaTi_{0.6}Al_{0.2}Nb_{0.2}OSiO_4$.
Note: the $P2_1/a$ model has a non-standard origin, offset by [0, ¼, ¼].

The volume of the XO_7 coordination polyhedron in the $Ca(Ti_{1-2x}Nb_xAl_x)OSiO_4$ series (Table 1) is similar to that in the $CaTiOSiO_4$ end member described by Kek *et al.* (1997) and Liferovich & Mitchell (2005b). The volume of the XO_7 coordination polyhedron in the $(Ca_{1-x}Na_x)(Ti_{1-x}Nb_x)OSiO_4$ is larger owing to entry of the larger Na^+ cation (Table 1).

The volume of the YO_6 coordination polyhedra in any Nb-doped titanite is larger than that in pure CaTi $OSiO_4$, and essentially does not change with *x* in the $(Ca_{1-x}Na_x)(Ti_{1-x}Nb_x)OSiO_4$ series, but demonstrates a stepwise decrease in the $Ca(Ti_{1-2x}Nb_xAl_x)OSiO_4$ series (Table 1).

The distortion index introduced by Shannon (1976) is useful to illustrate polyhedron bond-length distortion, *i.e.*, $\Delta_n = 1/n[\Sigma(r_i - \bar{r})/\bar{r}]^2 \bullet 10^3$, where r_i and $\bar{r}$ are individual and average bond-lengths in the polyhedron, respectively. The index of bond-length distortion is a measure of the distortion of polyhedra induced by compression–extension of cation–oxygen bonds resulting from stretching or compressional deformation, which induces violations in the ideal symmetry of an undistorted polyhedron. To characterize deviations from the ideal bond-angles in regular polyhedra, we calculate the bond-angle variance index, δ_n, where $\delta_n = [\Sigma(\theta_i - \theta_n)^2]/(n-1)$ and θ_i are the observed bond-angles at the central atom of a polyhedron, and θ_n is the ideal O–*M*–O or O–*T*–O angle in an undistorted polyhedron (Robinson *et al.* 1971). The bond-angle variance index reflects twisting and tilting deformation of coordination

polyhedra whose cation–oxygen distances may remain equal in length (Robinson *et al*. 1971), and thus remain similar in terms of bond-length variations. Both the Δ_n and δ_n distortion parameters provide specific insights into the complex geometrical distortions of given polyhedra.

Both the double-site and single-site substitutions induce an insignificant increase in the tetrahedral bond-length distortions as compared to Δ_4 in pure titanite (Table 1). In combination with the decrease of tetrahedron volume, this suggests that the tetrahedra, which serve as a bridging element of the framework structure, are compressed in the niobian varieties of titanite doped with slightly larger cations as compared to those in pure $CaTiOSiO_4$ end member. Comparison of the indices of tetrahedral bond-angle variance shows that the SiO_4 tetrahedra are less twisted and tilted in the $(Ca_{1-x}Na_x)(Ti_{1-x}Nb_x)OSiO_4$ series than in the $Ca(Ti_{1-2x}Nb_xAl_x)OSiO_4$ series (Table 1).

The Δ_7 and Δ_6 parameters (Table 1) show that doping of the titanite structure with Nb results in considerable decrease of bond-length distortions induced by stretching or compression of the seven- and six-fold coordination polyhedra as compared to XO_7 and YO_6 polyhedra in the pure $CaTiOSiO_4$ end-member. In part, further distortions of polyhedra do not occur because of the similarity of the average radii of the substituting cations to those of the cations being substituted. A decrease in the Δ_6 distortion of Nb-bearing titanite might be also explained by the stabilization of the *A*2/*a* dimorph, which results from the centering or pseudo-centering of the *Y* cation in the octahedra. The latter might be facilitated by minimizing the second-order Jahn–Teller effect occurring around an $^{VI}Y^{4+}$ cation (Kunz & Brown 1994), or by relief of underbonding of bridging O(1) anions at antiphase boundaries (Hughes *et al*. 1997). The kinking of the chains of octahedra in Nb-bearing synthetic titanite, as illustrated by the pivoting *Y*–O(1)–*Y* angle (Table 1), does not differ significantly from that in the $CaTiOSiO_4$ end member in the $(Ca_{1-x}Na_x)(Ti_{1-x}Nb_x)OSiO_4$ solid-solution series and gradually increases with *x* in the $Ca(Ti_{1-2x}Nb_xAl_x)OSiO_4$ solid-solution series.

TABLE 3. SELECTED BOND-LENGTHS IN STOICHIOMETRIC TITANITE AND Nb-DOPED SYNTHETIC TITANITE

	$CaTiOSiO_4$*		$NaNb_1$	$NaNb_2$	$AlNb_1$	$AlNb_2$
Ca-O1	2.275(1)	*X*-O1	2.275(6)	2.311(7)	2.265(5)	2.284(6)
Ca-O2	2.430(1)	2× *X*-O2	2.415(4)	2.430(5)	2.400(4)	2.411(4)
Ca-O3	2.409(1)	2× *X*-O3	2.440(4)	2.471(5)	2.444(4)	2.465(4)
Ca-O4	2.405(1)	2× *X*-O3'	2.619(5)	2.607(6)	2.613(4)	2.599(5)
Ca-O4'	2.673(1)					
Ca-O5	2.423(1)					
Ca-O5'	2.581(1)					
Ti-O1	1.756(1)	2× *Y*-O1	1.874(2)	1.864(2)	1.869(2)	1.863(2)
Ti-O1'	1.988(1)	2× *Y*-O2	2.015(4)	2.018(4)	2.017(3)	2.013(4)
Ti-O2	1.991(1)	2× *Y*–O3	2.037(4)	2.040(4)	2.026(3)	2.014(4)
Ti–O3	1.984(1)					
Ti–O4	2.012(1)					
Ti–O5	2.023(1)					
Si-O2	1.646(1)	2× Si-O2	1.614(4)	1.605(5)	1.606(4)	1.610(4)
Si-O3	1.645(1)	2× Si-O3	1.628(5)	1.622(6)	1.629(5)	1.632(6)
Si-O4	1.647(1)					
Si-O5	1.651(1)					

* Synchrotron radiation data for $P2_1/a$-structured $CaTiSiO_5$ (Kek *et al*. 1997).
Nb-doped synthetic titanite: $NaNb_1$: $Ca_{0.9}Na_{0.1}Ti_{0.9}Nb_{0.1}OSiO_4$; $NaNb_2$: $Ca_{0.8}Na_{0.2}Ti_{0.8}Nb_{0.2}OSiO_4$; $AlNb_1$: $CaTi_{0.8}Nb_{0.1}Al_{0.1}OSiO_4$; $AlNb_2$: $CaTi_{0.6}Nb_{0.2}Al_{0.2}OSiO_4$.

Conclusions

The crystal-structure response to the substitution of $^{VI}Nb^{5+}$ for $^{VI}Ti^{4+}$ in titanite has been studied in the $(Ca_{1-x}Na_x)(Ti_{1-x}Nb_x)OSiO_4$ and $Ca(Ti_{1-2x}Nb_xAl_x)OSiO_4$ solid-solution series synthesized by ceramic methods at ambient pressure, with quenching in air. Our findings demonstrate that (OH,F)-free titanite varieties doped with Nb *via* both a single-site and a complex two-site schemes of substitution at $x = 0.1$ and 0.2 adopt the *A*2/*a* space group and are stable at ambient pressure and temperature. Both the single-site and two-site schemes of substitution affect the coherency of the off-centering of the ^{VI}Y atoms in the chains of octahedra and result in an antiferroelectric-to-paraelectric transition (Speer & Gibbs 1976, Ghose *et al*. 1991, Van Heurk *et al*. 1991, Kek *et al*. 1997). In part, our study confirms the previously published data for a phase transition driven by replacement of ≥0.05 *apfu* $^{VII}Ca^{2+}$ and 0.05 *apfu* $^{VI}Ti^{4+}$ (Hughes *et al*. 1997) or in the range of 0.09–0.18 *apfu* $^{VI}Ti^{4+}$ and $O(1)^{2-}$ by $^{VI}(Al,Fe)^{3+}$ and $(OH,F)^-$ (Troitzsch *et al*. 1999). Nevertheless, any conclusions on the nature of the centering of the ^{VI}Y atom in Nb-rich titanite, and thus discrimination between the *A*2/*a*-structured β and γ phases introduced by Troitzsch & Ellis (2002), are not possible on the basis of the routine X-ray powder-diffraction technique.

The extent of stretching of the seven-fold coordination polyhedra and octahedra decreases with entry of Nb in titanite structure, in comparison with those in pure $CaTiOSiO_4$. Deformations of octahedra induced by tilting and twisting are 4–5 times less in the Nb-doped titanite varieties than in pure $CaTiOSiO_4$. The SiO_4 tetrahedron is compressed and more tilted and twisted in the Nb-doped titanite varieties than in pure $CaTiOSiO_4$.

The empirical limit for entry of Nb to the (F,OH)-free titanite structure at ambient pressure is ~0.25 *apfu* Nb in Nb–Al titanite (*ca*. 16.5 wt.% Nb_2O_5) and ~0.22 *apfu* Nb in Na–Nb titanite. The limit may probably be greater in natural varieties of titanite, where contiguous substitutions involving for example, $OH^- + F^-$ at the O(1) site or vacancies at cation sites, can occur.

The experimental data suggest that the existence of a titanite analogue with more than 50 mol.% of the $NaNbOSiO_4$ end member is unlikely. The solid solution

involving the smaller $^{VI}(Al_{0.5},Nb_{0.5})$ cations theoretically might be stabilized at high pressure, suggesting the existence of a potentially new species with dominance of the $Ca(Al_{0.5}Nb_{0.5})OSiO_4$ end member, as has been proposed by Černý *et al*. (1995) for analogs of titanite enriched in (Nb,Ta).

The tolerance of the titanite structure to entry of Nb implies that the compositions of synthetic titanite might be suitable for the sequestration of radioactive waste containing ^{94}Nb and other isotopes of Nb.

Acknowledgements

This work is supported by the Natural Sciences and Engineering Research Council of Canada and Lakehead University (Canada). We are grateful to Allan MacKenzie for assistance with the analytical work, and Anne Hammond for sample preparation. The comments and suggestions of Sergey Krivovichev, an anonymous reviewer and Robert F. Martin helped to improve the initial version of manuscript. Carlo Aurisicchio and Robert F. Martin are thanked for editorial handling of the manuscript.

References

Angel, R.J., Kunz, M., Miletich, R., Woodland, A.B., Koch, M. & Xirochakis, D. (1999): High-pressure phase transitions in $CaTiOSiO_4$ titanite. *Phase Trans*. **68**, 533-543.

Balić-Žunić, I.T. & Vicković, I. (1996): IVTON – a program for the calculations of geometrical aspects of crystal structures and some crystal chemical applications. *J. Appl. Crystallogr.* **29**, 305-306.

Brigatti, M.F., Caprilli, E., Mottana, A. & Poppi, L. (2004): Nb-containing titanite: new data and crystal structure refinement. *Neues Jahrb. Mineral., Monatsh.*, 117-126.

Černý, P., Novák, M. & Chapman, R. (1995): The Al(Nb,Ta)Ti_{-2} substitutions in titanite: the emergence of a new species? *Mineral. Petrol*. **52**, 61-73.

Černý, P. & Riva di Sanseverino, L. (1972): Comments on crystal chemistry of titanite. *Neues Jahrb. Mineral., Monatsh*. 97-103.

Chakhmouradian, A.R. (2004): Crystal chemistry and paragenesis of compositionally-unique (Al-, Fe-, Nb-, and Zr-rich) titanite from Afrikanda, Russia. *Am. Mineral*. **89**, 1752-1762.

Chakhmouradian, A.R., Reguir, E.P. & Mitchell, R.H. (2003): Titanite in carbonatitic rocks: genetic dualism and geochemical significance. *Per. Mineral*. **72**, Special Issue Eurocarb., 107-113.

Chakhmouradian, A.R. & Zaitsev, A.N. (2002): Calcite – amphibole – clinopyroxene rock from Afrikanda Complex, Kola Peninsula, Russia: mineralogy and possible link to carbonatites. III. Silicate minerals. *Can. Mineral*. **40**, 1347-1374.

Chiari, C., Gazzoni, G., Craig, J.R., Gibbs, G.V. & Louisnathan, S.J. (1985): Two independent refinements of the structure of paracelsian, $BaAl_2Si_2O_8$. *Am. Mineral*. **70**, 969-974.

Chrosch, J., Bismayer, U. & Salje, E.K.H. (1997): Antiphase boundaries and phase transitions in titanite: an X-ray diffraction study. *Am. Mineral*. **82**, 677-681.

Della Ventura, G., Bellatreccia, F. & Williams, C.T. (1999): Zr- and LREE-rich titanite from Tre Croci, Vico Volcanic complex (Latium, Italy). *Mineral. Mag*. **63**, 123-130.

Dowty, E. (1999): Atoms 5.0. Shape Software, Kingsport, Tennessee 37663, USA; http://shapesoftware.com/

Ghose, S., Ito, Y. & Hatch, D.M. (1991): Paraelectric–antiferroelectric phase transition in titanite, $CaTiSiO_5$. I. A high-temperature X-ray diffraction study of the order parameter and transition mechanism. *Phys. Chem. Minerals* **17**, 591-603.

Ghose, S., McMullan, R.K. & Weber, H.P. (1993): Neutron diffraction studies of the $P\bar{1}$ – $I\bar{1}$ transition in anorthite ($CaAl_2Si_2O_8$) and the crystal structure of the body-centered phase at 514 K. *Z. Kristallogr*. **204**, 215-237.

Griffen, D.T., Ribbe, P.H. & Gibbs, G.V. (1977): The structure of slawsonite, a strontium analog of paracelsian. *Am. Mineral*. **62**, 31-35.

Higgins, J.B. & Ribbe, P.H. (1976): The crystal chemistry and space groups of natural and synthetic titanites. *Am. Mineral*. **61**, 878-888.

Hollabaugh, C.L. & Foit, F.F., Jr. (1984): The crystal structure of an Al-rich titanite from Grisons, Switzerland. *Am. Mineral*. **69**, 725-732.

Hughes, J.M., Bloodaxe, E.S., Hanchar, J.M. & Foord, E.E. (1997): Incorporation of rare earth elements in titanite: stabilization of the *A*2/*a* dimorph by creation of antiphase boundaries. *Am. Mineral*. **82**, 512-516.

Kek, S., Aroyo, M., Bismayer, U., Schmidt, C., Eichhorn, K. & Krane, H.G. (1997): The two-step phase transition of titanite, $CaTiSiO_5$: a synchrotron radiation study. *Z. Kristallogr.* **212**, 9-19.

Kern, A.A. & Coelho, A.A. (1998): Topas. Allied Publishers Ltd., http://www.bruker-axs.com.

Kunz, M., Arlt, T. & Stolz, J. (2000): In situ powder diffraction study of titanite ($CaTiOSiO_4$) at high pressure and high temperature. *Am. Mineral*. **85**, 1465-1473.

Kunz, M. & Brown, I.D. (1994): Out-of-center distortions around octahedrally coordinated d^0-transition metals. *J. Solid State Chem*. **115**, 395-406.

KUNZ, M., XIROUCHAKIS, D., LINDSLEY, D.H. & HÄUSERMANN, D. (1996): High-pressure phase transition in titanite ($CaTiOSiO_4$). *Am. Mineral.* **81**, 1527-1530.

LIFEROVICH, R.P., LOCOCK, A.J., MITCHELL, R.H. & SHPACHENKO, A.K. (2006): The crystal structure of stronalsite and a redetermination of the structure of banalsite. *Can. Mineral.* **44**, 533-546.

LIFEROVICH, R.P. & MITCHELL, R.H. (2005a): Composition and paragenesis of Na-, Nb- and Zr-bearing titanite from Khibina, Russia, and crystal-structure data for synthetic analogues. *Can. Mineral.* **43**, 795-812.

LIFEROVICH, R.P. & MITCHELL, R.H. (2005b): Solid solution of rare earth elements in synthetic titanite: a reconaissance study. *Mineral. Petrol.* **83**, 271-282.

MAKOVICKY, E. & BALIĆ-ZUNIĆ, T. (1998): New measure of distortion for coordination polyhedra. *Acta Crystallogr.* **B54**, 766-773.

MALCHEREK, T. (2001): Spontaneous strain in synthetic titanite, $CaTiOSiO_4$. *Mineral. Mag.* **65**, 709-715.

MONGIORGI, R. & RIVA DI SANSEVERINO, L.R. (1968): A reconsideration of the structure of titanite, $CaTiOSiO_4$. *Mineral. Petrogr. Acta* **14**, 123-141.

PAUL, B.J., ČERNÝ, P., CHAPMAN, R. & HINTHORNE, J.R. (1981): Niobian titanite from the Huron claim pegmatite, southeastern Manitoba. *Can. Mineral.* **19**, 549-552.

ROBINSON, K., GIBBS, G.V. & RIBBE, P.H. (1971): Quadratic elongation: a quantitative measure of distortion in coordination polyhedra. *Science* **172**, 567-570.

ROSSI, G., OBERTI, R. & SMITH, D.C. (1986): Crystal structure of lisetite, $CaNa_2Al_4Si_4O_{16}$. *Am. Mineral.* **71**, 1378-1383.

SAHAMA, T.G. (1946): On the chemistry of mineral titanite. *C.R. Soc. Géol. Finlande* 19, **139**, 88-120.

SALJE, E., SCHMIDT, C. & BISMAYER, U. (1993): Structural phase transitions in titanite, $CaTiSiO_5$: a Raman spectroscopic study. *Phys. Chem. Minerals* **19**, 502-506.

SAWKA, W.N., CAMPBELL, R.B. & NORRISH, K. (1984): Light-rare-earth-element zoning in sphene and allanite during granitoid fractionation. *Geology* **12**, 131-134.

SHANNON, R.D. (1976): Revised effective ionic radii and systematic studies of interatomic distances in halides and chalcogenides. *Acta Crystallogr.* **A32**, 751-767.

SPEER, J.A. & GIBBS, G.V. (1976): The crystal structure of synthetic titanite, $CaTiOSiO_4$, and the domain textures of natural titanites. *Am. Mineral.* **61**, 238-247.

TAIT, K.T., SOKOLOVA, E., HAWTHORNE, F.C. & KHOMYAKOV, A.P. (2003): The crystal chemistry of nepheline. *Can. Mineral.* **41**, 61-70.

TAYLOR, M. & BROWN, G.E. (1976): High-temperature structural study of the $P2_1/a \leftrightarrow A2/a$ phase transition in synthetic titanite, $CaTiSiO_5$. *Am. Mineral.* **61**, 435-447.

TIEPOLO, M., OBERTI, R. & VANUCCI, R. (2002): Trace-element incorporation in titanite: constraints from experimentally determined solid/liquid partition coefficients. *Chem. Geol.* **191**, 105-119.

TROITZSCH, U. & ELLIS, D.J. (2002): Thermodynamic properties and stability of AlF-bearing titanite $CaTiOSiO_4$–$CaAlFSiO_4$. *Contrib. Mineral. Petrol.* **142**, 543-563.

TROITZSCH, U., ELLIS, D.J., THOMPSON, J. & FITZGERALD, J.D. (1999): Crystal-structural changes in titanite along the join TiO–AlF. *Eur. J. Mineral.* **11**, 955-965.

VAN HEURK, C., VAN TENDELOO, G., GHOSE, S. & AMELINCKX, S. (1991): Paraelectric–antiferroelectric phase transition in titanite, $CaTiSiO_5$. II. Electron diffraction and electron microscopic studies of the transition dynamics. *Phys. Chem. Minerals* **17**, 604-610.

WAINWRIGHT, J.E. & STARKEY, J. (1971): A refinement of the structure of anorthite. *Z. Kristallogr.* **133**, 75-84.

Received April 23, 2005, revised manuscript accepted March 3, 2006.